https://doi.org/10.5194/gmd-2022-227
Preprint. Discussion started: 19 September 2022

Geoscientific Model Development
Discussions

Implementation of trait-based ozone plant sensitivity in the Yale Interactive terrestrial Biosphere model v1.0 to assess global vegetation damage

Yimian Ma [1, 2], Xu Yue [3*], Stephen Sitch [4*], Nadine Unger [3], Johan Uddling [5], Lina M. Mercado [4, 6], Cheng Gong [7], Zhaozhong Feng [8], Huiyi Yang [9], Hao Zhou [1, 2], Chenguang Tian [1, 2], Yang Cao [1, 2], Yadong Lei [10], Alexander W. Cheesman [4, 11], Yansen Xu [8], Maria Carolina Duran Rojas [12]

[1] Climate Change Research Center, Institute of Atmospheric Physics, Chinese Academy of Sciences, Beijing, 100029, China
[2] University of Chinese Academy of Sciences, Beijing, 100029, China
[3] Jiangsu Key Laboratory of Atmospheric Environment Monitoring and Pollution Control, Jiangsu Collaborative Innovation Center of Atmospheric Environment and Equipment Technology, School of Environmental Science and Engineering, Nanjing University of Information Science and Technology, Nanjing, 210044, China
[4] Faculty of Environment, Science and Economy, University of Exeter, Exeter, EX4 4RJ, UK
[5] Department of Biological and Environmental Sciences, University of Gothenburg, Gothenburg, P.O. Box 461, 40530, Sweden
[6] UK Centre for Ecology and Hydrology, Benson Lane, Wallingford, OX10 8BB, UK
[7] State Key Laboratory of Atmospheric Boundary Layer Physics and Atmospheric Chemistry (LAPC), Institute of Atmospheric Physics, Chinese Academy of Sciences, Beijing, 100029, China
[8] School of Applied Meteorology, Nanjing University of Information Science and Technology, Nanjing, 210044, China
[9] Livelihoods and Institutions Department, Natural Resources Institute, University of Greenwich, Kent, ME4 4TB, UK
[10] Chinese Academy of Meteorological Sciences, Beijing, 100081, China
[11] Centre for Tropical Environmental and Sustainability Science, College of Science & Engineering, James Cook University, Cairns, Queensland, 4870 Australia
[12] College of Engineering, Mathematics, and Physical Sciences, University of Exeter, Exeter, EX4 4PY, UK

Correspondence to: Xu Yue (yuexu@nuist.edu.cn) and Stephen Sitch (S.A.Sitch@exeter.ac.uk)

https://doi.org/10.5194/gmd-2022-227
Preprint. Discussion started: 19 September 2022

Geoscientific Model Development
Discussions

Abstract

A major limitation in modeling global ozone (O_3) vegetation damage has long been the reliance on empirical O_3 sensitivity parameters derived from a limited number of species and applied at the level of plant functional types (PFTs), which ignore the large interspecific variations within the same PFT. Here, we present a major advance in large-scale assessments of O_3 plant injury by linking the trait leaf mass per area (LMA) and plant O_3 sensitivity in a broad and global perspective. Application of the new approach and a global LMA map in a dynamic global vegetation model reasonably represents the observed interspecific responses to O_3 with a unified sensitivity parameter for all plant species. Simulations suggest a contemporary global mean reduction of 4.8% in gross primary productivity by O_3, with a range of 1.1%-12.6% for varied PFTs. Hotspots with damages > 10% are found in agricultural areas in the eastern U.S., western Europe, eastern China, and India, accompanied by moderate to high levels of surface O_3. Furthermore, we simulate the distribution of plant sensitivity to O_3, which is highly linked with the inherent leaf trait trade-off strategies of plants, revealing high risks for fast-growing species with low LMA, such as crops, grasses and deciduous trees.

https://doi.org/10.5194/gmd-2022-227
Preprint. Discussion started: 19 September 2022

Geoscientific Model Development Discussions

1. Introduction

Tropospheric ozone (O_3) has long been recognized as a hazardous pollutant for plants (Reich and Amundson, 1985; Richards et al., 1958). As a strong oxidant, O_3 can cause damage to leaf cells and modulate the carbon balance of ecosystems through both direct and indirect impacts on plant function (Ainsworth et al., 2012; Feng et al., 2014; Wittig et al., 2009). To date, O_3 fumigation experiments have revealed a large variation in O_3 sensitivities among and within plant functional types (PFTs) (Buker et al., 2015; Mills et al., 2018a) (Table S1). Generally, needleleaf trees, deciduous woody plants, and crop species show ascending sensitivities to O_3 (Buker et al., 2015; Davison and Barnes, 1998; Reich and Amundson, 1985). The cause of such variation is not fully understood and thus has not been uniformly described in vegetation models (Massman et al., 2000; Tiwari et al., 2016). As a result, large-scale assessments of O_3 vegetation damage have to rely on a PFT-based range of sensitivity parameters derived from a limited number of plant species (Felzer et al., 2009; Lombardozzi et al., 2015; Sitch et al., 2007). For example, Sitch et al. (2007) (hereafter S2007) attempted to envelop the range of O_3 impacts by assuming all species within a PFT are either "high" or "low" sensitive to O_3, which cannot resolve intra-PFT variations and thus may cause large uncertainties in regional to global assessments.

Recent observations revealed a uniform plant sensitivity to O_3 if stomatal O_3 flux is expressed based on leaf mass rather than leaf area (Feng et al., 2018; Li et al., 2016; Li et al., 2022). The trait of leaf mass per area (LMA) is an important metric linking leaf area to mass. In a comparative study with 21 woody species (Li et al., 2016) and a meta-analysis of available experimental data (Feng et al., 2018), the dose-response relationship (DRR) shows convergent O_3 sensitivities for conifer and broadleaf trees if the area-based stomatal uptake was converted to the mass-based flux with LMA. Meanwhile, a large number of trait observations were synthesized by global networks in recent decades (Gallagher et al., 2020). The TRY initiative (Kattge et al., 2011) is one of the most influential datasets with 2.3 billion trait data by the year 2021. Based on the TRY dataset, global LMA was estimated with upscaling techniques such as Bayesian modeling (Butler et al., 2017) (thereafter B2017) or the random forest model (Moreno-Martinez et al., 2018) (thereafter M2018). These advances in the retrieval of LMA provide the possibility to depict more accurate O_3 vegetation damage at the global scale.

https://doi.org/10.5194/gmd-2022-227
Preprint. Discussion started: 19 September 2022

Geoscientific Model Development Discussions

Here, we present a major advance in large-scale assessments of O_3 plant damage using a trait-based approach. We implement LMA into a stomatal flux-based O_3 damage framework aiming at a unified representation of plant O_3 sensitivities over the global grids. We couple this new approach to the Yale Interactive terrestrial Biosphere (YIBs) model (Yue and Unger, 2015) and evaluate the derived O_3 sensitivities against observations. We further assess contemporary O_3 impacts on global gross primary productivity (GPP) in combination with the recently developed LMA datasets (Butler et al., 2017; Gallagher et al., 2020; Moreno-Martinez et al., 2018) (Fig. S1a) and the multi-model ensemble mean surface O_3 concentrations (Fig. S1b). The updated risk map for O_3 vegetation damage is used to identify the regions and species with the largest sensitivity to O_3 threats.

2. Scheme development and calibration

2.1 The trait-based O_3 vegetation damage scheme

We develop the new scheme based on the S2007 framework for transient O_3 damage calculation. In the original S2007 scheme, the undamaged fraction F for net photosynthetic rate is dependent on the excessive area-based stomatal O_3 flux, which is calculated as the difference between f_{O3} and PFT-specific area-based threshold y, and modulated by the sensitivity parameter a_{PFT}:

$$F = 1 - a_{PFT} \times max\{f_{O3} - y, 0\} \quad (1)$$

where a_{PFT} is calibrated and varies among PFTs with a typical range from "low" to "high" values indicating uncertainties of plant species within the same PFT in Sitch et al. (2007). The stomatal O_3 flux f_{O3} is calculated as:

$$f_{O3} = \frac{[O_3]}{r + \left[\frac{k_{O3}}{g_p \times F}\right]} \quad (2)$$

where $[O_3]$ is the O_3 concentration at the reference level (nmol m^{-3}), r is the aerodynamic and boundary layer resistance between leaf surface and reference level (s m^{-1}). k_{O3} setting to 1.67 represents the ratio of

https://doi.org/10.5194/gmd-2022-227
Preprint. Discussion started: 19 September 2022

leaf resistance for O_3 to that for water vapor. g_p represents potential stomata conductance for H_2O (m s^{-1}).

Studies suggested that LMA could be used to unify the area-based plant sensitivities to O_3 (Feng et al., 2018; Li et al., 2016), resulting in a constant mass-based parameter a independent of plant species and PFTs:

$$a = a_{PFT} \times LMA \tag{3}$$

Here, we convert the area-based O_3 stomatal flux expression in Equation (1) to a mass-based flux as follows:

$$F = 1 - a \times \max\left\{\frac{f_{O3}}{LMA} - x, 0\right\} \tag{4}$$

where the new sensitivity parameter a is a cross-species constant (nmol^{-1} s g); LMA is leaf mass per area (g m^{-2}); the flux threshold is replaced by a mass-based value of x (nmol g^{-1} s^{-1}) (Feng et al., 2018). This equation is applied at the timestep of photosynthesis calculation in the YIBs model (i.e. hourly). The updated LMA-based framework (YIBs-LMA) reduces the number of O_3 sensitivity parameters from three for each PFT (Sitch et al., 2007) in S2007 to a single parameter a for all PFTs. For YIBs-LMA framework, the default value of the x threshold in Equation (4) is set to 0.019 nmol g^{-1} s^{-1} as recommended by Feng et al. (2018).

2.2 Dose-response relationship (DRR)

We compare the simulated and observed sensitivities to O_3 so as to calibrate the LMA-based scheme. In field experiments, DRR is used to quantify species-specific damage by O_3 with a generic format as follows:

$$R = 100 + S_O \times \phi_{O3} \tag{5}$$

where R (%) is the relative percentage of a bio-indicator (such as biomass or yield) after and before O_3 damage; ϕ_{O3} is an area-based O_3 metric (e.g., POD_y measured in sunlit leaves at the top of canopy); S_O (usually negative) is the observed sensitivity derived as the slope of linear relationship between R and ϕ_{O3}. We collected S_O from DRRs with conventional criteria (typically $POD_{y=1}$ for natural PFTs and $POD_{y=6}$ for crops as dose metrics (CLRTAP, 2017); the bio-indicators include the relative biomass for natural PFTs and relative yield for crops) among plant species from International Cooperative Programme

https://doi.org/10.5194/gmd-2022-227
Preprint. Discussion started: 19 September 2022

Geoscientific Model Development
Discussions

on Effects of Air Pollution on Natural Vegetation and Crops (CLRTAP) (CLRTAP, 2017) and multiple literature sources (Table S1). Such observations are used to calibrate the LMA-based scheme.

As a comparison with observations, we calculate annual relative GPP percentage (R_{GPP}, %) and POD_y of sunlit leaves in first canopy layer (mmol m^{-2} year^{-1}, based on per leaf area) from the vegetation model to derive the slopes (S_S) of simulated DRRs. Here, POD_y is a diagnostic variable calculated as:

$$POD_y = \int (f_{O3} - y) \tag{6}$$

where f_{O3} represents the stomatal O_3 flux under instant O_3 stimulus at each timestep, which can be calculated following Equation (2) on the leaf level; y is the prescribed critical level (1 nmol m^{-2} s^{-1} for natural or 6 nmol m^{-2} s^{-1} for crop species (CLRTAP, 2017)). Excessive O_3 flux above y is accumulated for the top canopy layer and over the growing season to derive the POD_y. Simulated S_S is calculated as the slope of regression between simulated R_{GPP} (%) and POD_y at the PFT level. Only the dominant PFT in each grid is considered for the estimate of S_S at both PFT-level or gridded analyses.

Similarly, mass-based POD_x is derived from O_3 impacted f_{O3} (nmol m^{-2} s^{-1}) in Equation (2), together with gridded LMA (g m^{-2}) and mass-based threshold x (nmol g^{-1} s^{-1}) as:

$$POD_x = \int \left(\frac{f_{O3}}{LMA} - x\right) \tag{7}$$

2.3 Simulations and calibrations

We perform two groups of supporting experiments (Table 1). The first group explores modeling uncertainties associated with the mass-based framework: (1) YIBs-LMA_B2017 replaces the default LMA map of M2018 (Moreno-Martinez et al., 2018) with B2017 (Butler et al., 2017). (2) YIBs-LMA_PFT applies PFT-specific LMA values (Table S2) for each PFT without considering global LMA geo-gradient. (3) YIBs-LMA_T replaces the default threshold of x=0.019 nmol g^{-1} s^{-1} with x =0.006 nmol g^{-1} s^{-1}, which is an alternative parameter suggested by observations (Feng et al., 2018). The second group of supporting experiments explores the differences between mass-based and S2007 area-based

https://doi.org/10.5194/gmd-2022-227
Preprint. Discussion started: 19 September 2022

frameworks. Typically, S2007 has a "low to high" a_{PFT} range for each PFT. Here, a mean sensitivity parameterization of S2007 (YIBs-S2007_adj) is re-calibrated according to S_O in Table S1.

For all supporting experiments, the parameter a for YIBs-LMA or the eight mean a_{PFT} for YIBs-S2007_adj are derived with the optimal 1:1 fitting between S_S and S_O to minimize the possible biases (Tables S3-S7). Since S_O are available only for six out of the eight YIBs PFTs, including EBF, NF, DBF, C_3 grass, C_4 grass, and crop (Table S1), S_O of these PFTs are used for calibration.

2.4 YIBs model and forcing data

In this study, all O_3 vegetation damage schemes are implemented in the YIBs model (Yue and Unger, 2015). The YIBs is a process-based dynamic global vegetation model incorporated with well-established carbon, energy, and water interactive schemes. The model applies the same PFT classifications as the Community Land Model (Bonan et al., 2003) (Fig. S2). Eight PFTs are employed including evergreen broadleaf forest (EBF), needleleaf forest (NF), deciduous broadleaf forest (DBF), cold shrub (C_SHR), arid shrubland (A_SHR), C_3 grassland (C3_GRA), C_4 grassland (C4_GRA), and cropland (CRO) (Fig. S2). For each PFT, phenology is well-evaluated (Yue and Unger, 2015) to generate a reliable growing season, which is crucial for the simulation of stomatal O_3 uptake (Anav et al., 2018). Photosynthesis and stomatal processes are calculated using Farquhar et al. and Ball-Berry algorithms (Ball et al., 1987; Farquhar et al., 1980), respectively. Leaf area index (LAI) and tree height are predicted dynamically based on vegetation carbon allocation. The YIBs model has joined the multi-model ensemble project TRENDY and showed reasonable performance in the simulations of global biomass, GPP, LAI, net ecosystem exchange, and soil carbon relative to observations (Friedlingstein et al., 2020). Key plant biogeochemical parameters of the YIBs model are adjusted for this research (Table S8).

The hourly modern-era retrospective analysis for research and applications version 2 (MERRA2) climate reanalyses (Gelaro et al., 2017) are used to drive the YIBs model. The gridded LMA required for the main mass-based simulation is derived from Moreno-Martinez et al. (2018) (M2018), which shows the highest value of >150 g m^{-2} for needleleaf forest at high latitudes while low values of ~40 g m^{-2} for grassland and

https://doi.org/10.5194/gmd-2022-227
Preprint. Discussion started: 19 September 2022

Geoscientific Model Development Discussions

cropland (Fig. S1a and Fig. S2). Grids with missing LMA data are filled with the mean of the corresponding PFT. Contemporary O_3 concentration fields in the year of 2010 from the multi-model mean in Task Force on Hemispheric Transport of Air Pollutants (TF-HTAP) experiments (Turnock et al., 2018) (Fig. S1b) are used as forcing data. The original monthly O_3 data are downscaled to hourly using the diurnal cycle predicted by the chemistry-climate-carbon fully coupled model ModelE2-YIBs (Yue and Unger, 2015). All data are interpolated to the spatial resolution of 1º×1º.

3. Results

3.1 Comparison of simulated sensitivities with observations

Simulated relative GPP percentage (R_{GPP}) at global grids were sorted by dominant PFTs (Fig. S2) and plotted against area-based accumulated phytotoxic O_3 dose above a threshold y nmol m^{-2} s^{-1} ($POD_{y=1}$) at the corresponding grids (Fig. 1). The DRR shows varied slopes among different PFTs, resulting in a coefficient of determination (R^2) around 0.54 for all PFTs (Figs 1a-1c). We further calculated the mass-based accumulated phytotoxic O_3 dose above a threshold of 0.019 nmol g s^{-1} ($POD_{x=0.019}$) and compared it with R_{GPP}. The updated DRR showed convergent slopes and reached a high R^2 of 0.77 across all PFTs (Figs 1d-1f), suggesting that the mass-based scheme could better unify O_3 sensitivities among different PFTs.

We then calibrated the single, best-fit *a* value for YIBs-LMA framework by minimizing the absolute difference between simulated (S_S) and observed (S_O) slopes of O_3 DRR for all PFTs. With different *a* parameters, the YIBs-LMA framework yielded considerably high R^2 of ~1.0 but varied biases between simulated and observed O_3 impacts across PFTs (Fig. 2). Both the 1:1 fitting and the lowest bias between S_S and S_O were achieved with an optimal a =3.5 nmol^{-1} s g (Fig. 2c). Consistent with observations, YIBs-LMA with this optimal *a* parameter simulated low S_S of -0.18% and -0.36% per mmol m^{-2} year^{-1} of $POD_{y=1}$ for evergreen broadleaf forest and needleleaf forest, respectively (Figs 3a, b), median S_S from -0.53% per mmol m^{-2} year^{-1} for arid shrubland (Fig. 3e), and high S_S from -0.64% to -1.04% per mmol m^{-2} year^{-1} for deciduous broadleaf forest, C_3/C_4 grassland, cropland and cold shrubland (-3.28% for crops with $POD_{y=6}$, Figs 3c-d, 3f-h).

https://doi.org/10.5194/gmd-2022-227
Preprint. Discussion started: 19 September 2022

3.2 Global map of O_3 vegetation damage

We estimated contemporary GPP reductions induced by O_3 with the global concentrations of surface O_3 (Fig. S1b) in the year of 2010. The YIBs-LMA framework using an increase of *a* parameter yielded an almost linearly enhancement of global GPP reduction (Fig. S3) with consistent spatial distributions (Fig. S4). The simulation with the optimal a =3.5 nmol^{-1} s g predicted a global GPP reduction of 4.8% (Fig. 4a), which was similar to the value estimated with the area-based S2007 scheme (YIBs-S2007_adj, Table 1). Large reductions of >10% were predicted over eastern U.S., western Europe, eastern China, and India (Fig. 4a). Hotspots were mainly located in cropland and agricultural areas mixed with deciduous broadleaf forest or grassland, accompanied with moderate to high levels of surface O_3. Few discrepancies between the damage maps of YIBs-LMA and YIBs-S007_adj were found (Fig. 4b), even though the number of parameters was greatly reduced in YIBs-LMA scheme.

For YIBs-LMA, PFTs with low LMA such as cropland, grassland, and deciduous broadleaf forest account for 73.3 Pg C yr^{-1} (50.0%) of the global GPP (Table S9). However, these PFTs contributed to a total GPP reduction of 5.4 Pg C yr^{-1} (75.5% of total GPP loss) by O_3 damage. In contrast, evergreen broadleaf and needleleaf forests with high LMA accounted for 48.8 Pg C yr^{-1} (33.0%) of total GPP but yielded only a reduction of 0.75 Pg C yr^{-1} (10.5% of total GPP loss). Differences in GPP percentage losses were in part associated with the global pattern of O_3 concentrations, which were usually higher over mid-latitudes with populated cities and dense crop plantations (Fig. S1b). However, the differences in LMA and simulated O_3 sensitivities of these PFTs were the main cause of discrepancies in GPP damage at the large scale.

3.3 Uncertainties of the LMA-based scheme

We quantified the uncertainties of LMA-based shceme by comparing simulated GPP damages among different experiments (Table 1). The experiment with the alternative LMA map of B2017 (Fig. S5) showed a slightly enhanced GPP reduction of 5.3% (Fig. 5a) but similar spatial patterns compared with YIBs-LMA using M2018 (Fig. 4a). However, B2017 has a much less source of LMA data than M2018 (~40%), leading to some unexpected areas with high O_3 threats such as the tundra in Arctic region (Fig.

https://doi.org/10.5194/gmd-2022-227
Preprint. Discussion started: 19 September 2022

S6). The experiment with PFT-specific LMA estimated a global GPP reduction of 4.6% (Fig. 5b) with consistent spatial pattern as the prediction with YIBs-LMA, suggesting the reasonable application of PFT-level LMA at the lack of global LMA data. The experiment with an alternative threshold flux (Feng et al., 2018) of 0.006 nmol g^{-1} s^{-1} estimated a higher GPP reduction of 6.5% by global O_3 (Fig. 5c) with overestimations of O_3 sensitivities for some tree PFTs (Fig. 6). The YIBs-S2007_adj run using recalibrated PFT-level sensitivities predicts a similar global GPP damage of 4.8% as the YIBs-LMA run with a high spatial correlation coefficient of 0.98 (Fig. 5d). All sensitivity experiments achieve consistent results as the YIBs-LMA simulation with an uncertaintiy range from -0.2% to 1.7% and spatial correlation coefficients larger than 0.94.

4. Discussion

4.1 Mechanisms behind the LMA-based approach

In recent decades, the plant science community examined how traits could be used to differentiate and predict the functions of plant species (Reich et al., 1999; Reich et al., 1997). LMA, related to leaf density and thickness, is a key trait reflecting many aspects of leaf function (Reich et al., 1998). In the field of O_3 phytotoxicology, experiments have revealed plants with high LMA usually have thick leaves with physical and chemical defenses (Poorter et al., 2009), which can strengthen their resistance to O_3 (Feng et al., 2018; Li et al., 2016). On the contrary, plants with low LMA normally have thin leaves which are likely to be less O_3-tolerant (Feng et al., 2018; Li et al., 2016). Moreover, it seems plausible that the oxidative stress caused by a given amount of stomatal O_3 flux per unit leaf area would be distributed over a larger leaf mass, and hence diluted, in a leaf with high LMA. Such a LMA-O_3 sensitivity relationship can be well reproduced by our LMA-based model (Figs 7a and 7b). Below we explore the linkage between O_3 plant sensitivities and the mutual adaptation of growth strategies and leaf morphology with plant leaf trade-off theory (Reich et al., 1999; Shipley et al., 2006).

In the natural world, plants often adapt to maximize carbon uptake under prevailing conditions (Reich et al., 1998; Shipley et al., 2006). To make full use of resources in the growing season, leaves under varied living conditions choose either fast photosynthetic rates (fast-growing deciduous types) or long

https://doi.org/10.5194/gmd-2022-227
Preprint. Discussion started: 19 September 2022

photosynthesis duration (slow-growing evergreen types) with compatible leaf structures (Diaz et al., 2016; Reich, 2014). The former species expand leaf area (low LMA) to maximize light interception while the latter species produce thick and mechanically strong leaves (high LMA) with ample resistant substances for durable utilization (Poorter et al., 2009) in resource-limited and/or environment-stressed habitats (Wright et al., 2002). As a side effect of such leaf trade-offs, deciduous plants with their high rates of photosynthesis, associated large stomatal conductance (Davison and Barnes, 1998; Henry et al., 2019), and less total defense capacity through the leaf profile (Poorter et al., 2009), are highly O_3 sensitive (Mode1 in Fig. 8). In contrast, the moderate photosynthesis, relatively low maximum stomatal conductance (Davison and Barnes, 1998; Henry et al., 2019), and reinforced dense leaves (Poorter et al., 2009) lead to low sensitivity for evergreen plants (Mode2 in Fig. 8). Therefore, in our modelling practice, the mass-based O_3 gas exchange algorithm can be regarded as taking into account several interrelated factors such as growth-driven gas exchange requirements, gas path length and biochemical reserves, in a unified, simplified and effective manner via LMA.

4.2 Implication of potential risks for fast-growing plants

Our new approach reflected the general experimental findings that deciduous plants are much more vulnerable to O_3 than evergreen species (Feng et al., 2018; Li et al., 2017), and in turn within a PFT, early-successional/pioneers with low LMA are likely more vulnerable than late-successional/canopy trees with high LMA (Fyllas et al., 2012). This law has been neglected in previous modeling studies due to the dependence on the limited observed data used for PFT-specific tuning. Our LMA-based approach bridges this gap through grid-based parameterization, and in addition, our data-model integration specifically emphasizes the broad high risks for fast-growing plants, especially for crops. Among PFTs, crops may endure the largest O_3 threats (Davison and Barnes, 1998; Feng et al., 2021; Mukherjee et al., 2021) because they are artificially bred with high photosynthetic capacities (Richards, 2000), stomatal conductance, generally low LMA (Bertin and Gary, 1998; Li et al., 2018; Wang and Shangguan, 2010; Wu et al., 2018) (roughly 30-60 g m^{-2}), and cultivated in populated regions with high ambient O_3 concentrations. Modern technology aims to promote crop yield (Herdt, 2005), but this can potentially elevate crop sensitivities to O_3 (Biswas et al., 2013; Biswas et al., 2008). This study estimated the highest

https://doi.org/10.5194/gmd-2022-227
Preprint. Discussion started: 19 September 2022

annual mean GPP damage for crop, 12.6%, which is at the high end of the 4.4-12.4% of the O_3-induced yield loss estimated for global modeling of soybean, wheat, rice, and maize (Mills et al., 2018b). Furthermore, human-induced land use activities may also increase O_3 damage risks. The global demand for food and commodities leads to the conversion of natural forests to irrigated croplands, grazing pastures, and economical-tree plantations (Curtis et al., 2018; Zalles et al., 2021). Meanwhile, the urgent actions to combat climate change promote large-scale afforestation and reforestation (Cook-Patton et al., 2020). These land use changes with fast-growing plant species may increase the risks of terrestrial ecosystems to surface O_3.

4.3 Advances in the global O_3 damage assessment

For the first time, we implemented plant trait LMA into a process-based O_3 impact modeling scheme and obtained reasonable interspecific and inter-PFT O_3 responses supported by observations. This LMA-based approach indicates an important advance in global O_3 damage assessments. First, it significantly reduces the number of required key parameters. To account for interspecific sensitivities, many schemes have to define PFT-level parameters to cap the ranges of plant responses (Felzer et al., 2009; Lombardozzi et al., 2015; Sitch et al., 2007). As a result, those schemes rely on dozens of parameters which increase the uncertainties of modeling and the difficulties for model calibration. The LMA-based approach requires the calibration of one single parameter a, largely facilitating its application across different vegetation models. Second, the new approach accounts for the continuous spectrum of O_3 sensitivities. Previous studies usually categorized species into groups of low or high O_3 sensitivity, depending on very limited data from O_3 exposure experiments. As a result, gridcells for a specific PFT share the same sensitivities regardless of their geographic locations and ecosystem characteristics. In reality, there are hundreds and thousands of plant species in each PFT and they usually have large variation in biophysical parameters including LMA and O_3 sensitivities. The LMA-based approach takes advantage of the newly revealed unifying concept in O_3 sensitivity (Feng et al., 2018; Li et al., 2016; Li et al., 2022) and the recent development in a trait-based LMA global map (Fig. S1a). Such configurations present a spectrum of gridded O_3 sensitivities (Fig. 7a) following the variations of LMA and bring the possibility of capturing spatiotemporal variation in vegetation O_3 sensitivity through time-sensitive LMA products in the future.

https://doi.org/10.5194/gmd-2022-227
Preprint. Discussion started: 19 September 2022

Code availability

The codes of YIBs model with LMA-based O_3 damaging scheme are shared at https://zenodo.org/record/6348731.

Data availability

Results of all simulations (listed in Table 1) are available upon request. Data for Figures in the main article are shared at https://zenodo.org/record/6348731. The global maps of specific leaf area (SLA) to derive LMA for M2018 and B2017 are from https://www.try-db.org/TryWeb/Data.php#59 and https://github.com/abhirupdatta/global_maps_of_plant_traits, respectively. Monthly O_3 data is from https://doi.org/10.5194/acp-18-8953-2018. Calibration data are summarized in Table S1.

Author Contributions

X.Y., S.S. and N.U. designed the research, Y.M.M. performed modeling, data analyses, virtualization and wrote the draft. J.U, L.M., Z.Z.F, and A.W.C advised on concepts and methods. C.G. helped write draft. H.Y.Y., M.C.D.R helped with coding. H.Z., C.G.T., Y.C., Y.D.L., and Y.S.X. helped with data collection. All authors commented and revised the manuscript.

Competing interests

The authors declare no conflict of interests.

Financial support

Xu Yue acknowledges funding support from Jiangsu Science Fund for Distinguished Young Scholars (grant no. BK20200040). Yimian Ma acknowledges financial support from China Scholarship Council (CSC no. 201804910712). Johan Uddling acknowledges the strategic research area Biodiversity and Ecosystems in a Changing Climate, BECC. SS, NU, LM, AC were supported by NERC funding (NE/R001812/1).

https://doi.org/10.5194/gmd-2022-227
Preprint. Discussion started: 19 September 2022

Geoscientific Model Development Discussions
Open Access
EGU

References

Ainsworth, E. A., Yendrek, C. R., Sitch, S., Collins, W. J., and Emberson, L. D.: The Effects of Tropospheric Ozone on Net Primary Productivity and Implications for Climate Change, Annu Rev Plant Biol, 63, 637-661, 2012.

Anav, A., Liu, Q., De Marco, A., Proietti, C., Savi, F., Paoletti, E., and Piao, S.: The role of plant phenology in stomatal ozone flux modeling, Global Change Biol, 24, 235-248, 2018.

Ball, J. T., Woodrow, I. E., and Berry, J. A.: A model predicting stomatal conductance and its contribution to the control of photosynthesis under different environmental conditions, Progress in Photosynthesis Research: Viith International Congress on Photosynthesis, doi: 10.1007/978-94-017-0519-6_48, 1987. 1987.

Bertin, N. and Gary, C.: Short and long term fluctuations of the leaf mass per area of tomato plants - Implications for growth models, Ann Bot-London, 82, 71-81, 1998.

Biswas, D. K., Xu, H., Li, Y. G., Ma, B. L., and Jiang, G. M.: Modification of photosynthesis and growth responses to elevated CO2 by ozone in two cultivars of winter wheat with different years of release, J Exp Bot, 64, 1485-1496, 2013.

Biswas, D. K., Xu, H., Li, Y. G., Sun, J. Z., Wang, X. Z., Han, X. G., and Jiang, G. M.: Genotypic differences in leaf biochemical, physiological and growth responses to ozone in 20 winter wheat cultivars released over the past 60 years, Global Change Biol, 14, 46-59, 2008.

Bonan, G. B., Levis, S., Sitch, S., Vertenstein, M., and Oleson, K. W.: A dynamic global vegetation model for use with climate models: concepts and description of simulated vegetation dynamics, Global Change Biol, 9, 1543-1566, 2003.

Buker, P., Feng, Z., Uddling, J., Briolat, A., Alonso, R., Braun, S., Elvira, S., Gerosa, G., Karlsson, P. E., Le Thiec, D., Marzuoli, R., Mills, G., Oksanen, E., Wieser, G., Wilkinson, M., and Emberson, L. D.: New flux based dose-response relationships for ozone for European forest tree species, Environ. Pollut., 206, 163-174, 2015.

Butler, E. E., Datta, A., Flores-Moreno, H., Chen, M., Wythers, K. R., Fazayeli, F., Banerjee, A., Atkin, O. K., Kattge, J., Amiaud, B., Blonder, B., Boenisch, G., Bond-Lamberty, B., Brown, K. A., Byun, C., Campetella, G., Cerabolini, B. E. L., Cornelissen, J. H. C., Craine, J. M., Craven, D., de Vries, F. T., Diaz, S., Domingues, T. F., Forey, E., Gonzalez-Melo, A., Gross, N., Han, W., Hattingh, W. N., Hickler, T., Jansen, S., Kramer, K., Kraft, N. J. B., Kurokawa, H., Laughlin, D. C., Meir, P., Minden, V., Niinemets, U., Onoda, Y., Penuelas, J., Read, Q., Sack, L., Schamp, B., Soudzilovskaia, N. A., Spasojevic, M. J., Sosinski, E., Thornton, P. E., Valladares, F., van Bodegom, P. M., Williams, M., Wirth, C., and Reich, P. B.: Mapping local and global variability in plant trait distributions, Proc Natl Acad Sci U S A, 114, E10937-E10946, 2017.

CLRTAP: The UNECE Convention on Long-range Transboundary Air Pollution, Manual on Methodologies and Criteria for Modelling and Mapping Critical Loads and Levels and Air Pollution Effects, Risks and Trends: Chapter III Mapping Critical Levels for Vegetation, 2017. 2017.

Cook-Patton, S. C., Leavitt, S. M., Gibbs, D., Harris, N. L., Lister, K., Anderson-Teixeira, K. J., Briggs, R. D., Chazdon, R. L., Crowther, T. W., Ellis, P. W., Griscom, H. P., Herrmann, V., Holl, K. D., Houghton, R. A., Larrosa, C., Lomax, G., Lucas, R., Madsen, P., Malhi, Y., Paquette, A., Parker, J. D., Paul, K., Routh, D., Roxburgh, S., Saatchi, S., van den Hoogen, J., Walker, W. S., Wheeler, C. E., Wood, S. A., Xu, L., and Griscom, B. W.: Mapping carbon accumulation potential from global natural forest regrowth, Nature, 585, 545-550, 2020.

Curtis, P. G., Slay, C. M., Harris, N. L., Tyukavina, A., and Hansen, M. C.: Classifying drivers of global forest loss, Science, 361, 1108-1111, 2018.

Davison, A. W. and Barnes, J. D.: Effects of ozone on wild plants, New Phytol, 139, 135-151, 1998.

Diaz, S., Kattge, J., Cornelissen, J. H., Wright, I. J., Lavorel, S., Dray, S., Reu, B., Kleyer, M., Wirth, C., Prentice, I. C., Garnier, E., Bonisch, G., Westoby, M., Poorter, H., Reich, P. B., Moles, A. T., Dickie, J., Gillison, A. N., Zanne, A. E., Chave, J., Wright, S. J., Sheremet'ev, S. N., Jactel, H., Baraloto, C., Cerabolini, B., Pierce, S., Shipley, B., Kirkup, D., Casanoves, F., Joswig, J. S., Gunther, A., Falczuk, V., Ruger, N., Mahecha, M. D., and Gorne, L. D.: The global spectrum of plant form and function, Nature, 529, 167-171, 2016.

Farquhar, G. D., Caemmerer, S. V., and Berry, J. A.: A biochemical-model of photosynthetic CO_2 assimilation in leaves of C3 Species, Planta, 149, 78-90, 1980.

Felzer, B. S., Cronin, T. W., Melillo, J. M., Kicklighter, D. W., and Schlosser, C. A.: Importance of carbon-nitrogen interactions and ozone on ecosystem hydrology during the 21st century, J. Geophys. Res., 114, G01020, 2009.

Feng, Z., Agathokleous, E., Yue, X., Oksanen, E., Paoletti, E., Sase, H., Gandin, A., Koike, T., Calatayud, V., Yuan, X., Liu, X., De Marco, A., Jolivet, Y., Kontunen-Soppela, S., Hoshika, Y., Saji, H., Li, P., Li, Z., Watanabe, M., and Kobayashi, K.: Emerging challenges of ozone impacts on asian plants: actions are needed to protect ecosystem health, Ecosystem Health and Sustainability, 7, 1911602, 2021.

Feng, Z. Z., Buker, P., Pleijel, H., Emberson, L., Karlsson, P. E., and Uddling, J.: A unifying explanation for variation in ozone sensitivity among woody plants, Glob. Change Biol., 24, 78-84, 2018.

Feng, Z. Z., Sun, J. S., Wan, W. X., Hu, E. Z., and Calatayud, V.: Evidence of widespread ozone-induced visible injury on plants in Beijing, China, Environ Pollut, 193, 296-301, 2014.

Fyllas, N. M., Quesada, C. A., and Lloyd, J.: Deriving Plant Functional Types for Amazonian forests for use in vegetation dynamics models, Perspectives in Plant Ecology, Evolution and Systematics, 14, 97-110, 2012.

Gallagher, R. V., Falster, D. S., Maitner, B. S., Salguero-Gomez, R., Vandvik, V., Pearse, W. D., Schneider, F. D., Kattge, J., Poelen, J. H., Madin, J. S., Ankenbrand, M. J., Penone, C., Feng, X., Adams, V. M., Alroy, J., Andrew, S. C., Balk, M. A., Bland, L. M., Boyle, B. L.,

Bravo-Avila, C. H., Brennan, I., Carthey, A. J. R., Catullo, R., Cavazos, B. R., Conde, D. A., Chown, S. L., Fadrique, B., Gibb, H., Halbritter, A. H., Hammock, J., Hogan, J. A., Holewa, H., Hope, M., Iversen, C. M., Jochum, M., Kearney, M., Keller, A., Mabee, P., Manning, P., McCormack, L., Michaletz, S. T., Park, D. S., Perez, T. M., Pineda-Munoz, S., Ray, C. A., Rossetto, M., Sauquet, H., Sparrow, B., Spasojevic, M. J., Telford, R. J., Tobias, J. A., Violle, C., Walls, R., Weiss, K. C. B., Westoby, M., Wright, I. J., and Enquist, B. J.: Open Science principles for accelerating trait-based science across the Tree of Life, Nat Ecol Evol, 4, 294-303, 2020.
Gelaro, R., McCarty, W., Suarez, M. J., Todling, R., Molod, A., Takacs, L., Randles, C. A., Darmenov, A., Bosilovich, M. G., Reichle, R., Wargan, K., Coy, L., Cullather, R., Draper, C., Akella, S., Buchard, V., Conaty, A., da Silva, A. M., Gu, W., Kim, G.-K., Koster, R., Lucchesi, R., Merkova, D., Nielsen, J. E., Partyka, G., Pawson, S., Putman, W., Rienecker, M., Schubert, S. D., Sienkiewicz, M., and Zhao, B.: The Modern-Era Retrospective Analysis for Research and Applications, Version 2 (MERRA-2), J Climate, 30, 5419-5454, 2017.
Henry, C., John, G. P., Pan, R., Bartlett, M. K., Fletcher, L. R., Scoffoni, C., and Sack, L.: A stomatal safety-efficiency trade-off constrains responses to leaf dehydration, Nat Commun, 10, 3398, 2019.
Herdt, R. W.: The state of food and agriculture, 2003-2004: Agricultural biotechnology: Meeting the needs of the poor?, Agricultural Economics, 32, 109-+, 2005.
Kattge, J. and Diaz, S. and Lavorel, S. and Prentice, C. and Leadley, P. and Bonisch, G. and Garnier, E. and Westoby, M. and Reich, P. B. and Wright, I. J. and Cornelissen, J. H. C. and Violle, C. and Harrison, S. P. and van Bodegom, P. M. and Reichstein, M. and Enquist, B. J. and Soudzilovskaia, N. A. and Ackerly, D. D. and Anand, M. and Atkin, O. and Bahn, M. and Baker, T. R. and Baldocchi, D. and Bekker, R. and Blanco, C. C. and Blonder, B. and Bond, W. J. and Bradstock, R. and Bunker, D. E. and Casanoves, F. and Cavender-Bares, J. and Chambers, J. Q. and Chapin, F. S. and Chave, J. and Coomes, D. and Cornwell, W. K. and Craine, J. M. and Dobrin, B. H. and Duarte, L. and Durka, W. and Elser, J. and Esser, G. and Estiarte, M. and Fagan, W. F. and Fang, J. and Fernandez-Mendez, F. and Fidelis, A. and Finegan, B. and Flores, O. and Ford, H. and Frank, D. and Freschet, G. T. and Fyllas, N. M. and Gallagher, R. V. and Green, W. A. and Gutierrez, A. G. and Hickler, T. and Higgins, S. I. and Hodgson, J. G. and Jalili, A. and Jansen, S. and Joly, C. A. and Kerkhoff, A. J. and Kirkup, D. and Kitajima, K. and Kleyer, M. and Klotz, S. and Knops, J. M. H. and Kramer, K. and Kuhn, I. and Kurokawa, H. and Laughlin, D. and Lee, T. D. and Leishman, M. and Lens, F. and Lenz, T. and Lewis, S. L. and Lloyd, J. and Llusia, J. and Louault, F. and Ma, S. and Mahecha, M. D. and Manning, P. and Massad, T. and Medlyn, B. E. and Messier, J. and Moles, A. T. and Muller, S. C. and Nadrowski, K. and Naeem, S. and Niinemets, U. and Nollert, S. and Nuske, A. and Ogaya, R. and Oleksyn, J. and Onipchenko, V. G. and Onoda, Y. and Ordonez, J. and Overbeck, G. and Ozinga, W. A. and Patino, S. and Paula, S. and Pausas, J. G. and Penuelas, J. and Phillips, O. L. and Pillar, V. and Poorter, H. and Poorter, L. and Poschlod, P. and Prinzing, A. and Proulx, R. and Rammig, A. and Reinsch, S. and Reu, B. and Sack, L. and Salgado-Negre, B. and Sardans, J. and Shiodera, S. and Shipley, B. and Siefert, A. and Sosinski, E. and Soussana, J. F. and Swaine, E. and Swenson, N. and Thompson, K. and Thornton, P. and Waldram, M. and Weiher, E. and White, M. and White, S. and Wright, S. J. and Yguel, B. and Zaehle, S. and Zanne, A. E. and Wirth, C.: TRY - a global database of plant traits, Global Change Biol, 17, 2905-2935, 2011.
Li, D., Wang, X., Zheng, H., Zhou, K., Yao, X., Tian, Y., Zhu, Y., Cao, W., and Cheng, T.: Estimation of area- and mass-based leaf nitrogen contents of wheat and rice crops from water-removed spectra using continuous wavelet analysis, Plant Methods, 14, 2018.
Li, P., Calatayud, V., Gao, F., Uddling, J., and Feng, Z. Z.: Differences in ozone sensitivity among woody species are related to leaf morphology and antioxidant levels, Tree Physiol., 36, 1105-1116, 2016.
Li, P., Feng, Z., Catalayud, V., Yuan, X., Xu, Y., and Paoletti, E.: A meta-analysis on growth, physiological, and biochemical responses of woody species to ground-level ozone highlights the role of plant functional types, Plant Cell Environ, 40, 2369-2380, 2017.
Li, S., Moller, C. A., Mitchell, N. G., Lee, D., Sacks, E. J., and Ainsworth, E. A.: Testing unified theories for ozone response in C-4 species, Global Change Biol, 28, 3379-3393, 2022.
Lombardozzi, D., Levis, S., Bonan, G., Hess, P. G., and Sparks, J. P.: The Influence of Chronic Ozone Exposure on Global Carbon and Water Cycles, J Climate, 28, 292-305, 2015.
Massman, W. J., Musselman, R. C., and Lefohn, A. S.: A conceptual ozone dose-response model to develop a standard to protect vegetation, Atmos Environ, 34, 745-759, 2000.
Mills, G., Sharps, K., Simpson, D., Pleijel, H., Broberg, M., Uddling, J., Jaramillo, F., Davies, W. J., Dentener, F., Van den Berg, M., Agrawal, M., Agrawal, S. B., Ainsworth, E. A., Buker, P., Emberson, L., Feng, Z. Z., Harmens, H., Hayes, F., Kobayashi, K., Paoletti, E., and Van Dingenen, R.: Ozone pollution will compromise efforts to increase global wheat production, Global Change Biol, 24, 3560-3574, 2018a.
Mills, G., Sharps, K., Simpson, D., Pleijel, H., Frei, M., Burkey, K., Emberson, L., Uddling, J., Broberg, M., Feng, Z., Kobayashi, K., and Agrawal, M.: Closing the global ozone yield gap: Quantification and cobenefits for multistress tolerance, Glob Chang Biol, 24, 4869-4893, 2018b.
Moreno-Martinez, A., Camps-Valls, G., Kattge, J., Robinson, N., Reichstein, M., van Bodegom, P., Kramer, K., Cornelissen, J. H. C., Reich, P., Bahn, M., Niinemets, U., Penuelas, J., Craine, J. M., Cerabolini, B. E. L., Minden, V., Laughlin, D. C., Sack, L., Allred, B., Baraloto, C., Byun, C., Soudzilovskaia, N. A., and Running, S. W.: A methodology to derive global maps of leaf traits using remote sensing and climate data, Remote Sens Environ, 218, 69-88, 2018.
Mukherjee, A., Yadav, D. S., Agrawal, S. B., and Agrawal, M.: Ozone a persistent challenge to food security in India: Current status and policy implications, Current Opinion in Environmental Science & Health, 19, 100220, 2021.

https://doi.org/10.5194/gmd-2022-227
Preprint. Discussion started: 19 September 2022

Poorter, H., Niinemets, U., Poorter, L., Wright, I. J., and Villar, R.: Causes and consequences of variation in leaf mass per area (LMA): a meta-analysis, New Phytol, 182, 565-588, 2009.

Reich, P. B.: The world-wide 'fast-slow' plant economics spectrum: a traits manifesto, J Ecol, 102, 275-301, 2014.

Reich, P. B. and Amundson, R. G.: AMBIENT LEVELS OF OZONE REDUCE NET PHOTOSYNTHESIS IN TREE AND CROP SPECIES, Science, 230, 566-570, 1985.

Reich, P. B., Ellsworth, D. S., and Walters, M. B.: Leaf structure (specific leaf area) modulates photosynthesis-nitrogen relations: evidence from within and across species and functional groups, Funct Ecol, 12, 948-958, 1998.

Reich, P. B., Ellsworth, D. S., Walters, M. B., Vose, J. M., Gresham, C., Volin, J. C., and Bowman, W. D.: Generality of leaf trait relationships: A test across six biomes, Ecology, 80, 1955-1969, 1999.

Reich, P. B., Walters, M. B., and Ellsworth, D. S.: From tropics to tundra: Global convergence in plant functioning, P Natl Acad Sci USA, 94, 13730-13734, 1997.

Richards, B. L., Middleton, J. T., and Hewitt, W. B.: Air Pollution With Relation to Agronomic Crops: V. Oxidant Stipple of Grape, Agron J, 50, 559-561, 1958.

Richards, R. A.: Selectable traits to increase crop photosynthesis and yield of grain crops, J Exp Bot, 51, 447-458, 2000.

Shipley, B., Lechowicz, M. J., Wright, I., and Reich, P. B.: Fundamental trade-offs generating the worldwide leaf economics spectrum, Ecology, 87, 535-541, 2006.

Sitch, S., Cox, P. M., Collins, W. J., and Huntingford, C.: Indirect radiative forcing of climate change through ozone effects on the land-carbon sink, Nature, 448, 791-794, 2007.

Tiwari, S., Grote, R., Churkina, G., and Butler, T.: Ozone damage, detoxification and the role of isoprenoids - new impetus for integrated models, Funct Plant Biol, 43, 324-336, 2016.

Turnock, S. T., Wild, O., Dentener, F. J., Davila, Y., Emmons, L. K., Flemming, J., Folberth, G. A., Henze, D. K., Jonson, J. E., Keating, T. J., Kengo, S., Lin, M., Lund, M., Tilmes, S., and O'Connor, F. M.: The impact of future emission policies on tropospheric ozone using a parameterised approach, Atmos Chem Phys, 18, 8953-8978, 2018.

Wang, K. and Shangguan, Z.: Photosynthetic characteristics and resource utilization efficiency of maize (Zea maysL.) and millet (Setaria italicaL.) in a semi-arid hilly loess region in China, New Zeal J Crop Hort, 38, 247-254, 2010.

Wittig, V. E., Ainsworth, E. A., Naidu, S. L., Karnosky, D. F., and Long, S. P.: Quantifying the impact of current and future tropospheric ozone on tree biomass, growth, physiology and biochemistry: a quantitative meta-analysis, Global Change Biol, 15, 396-424, 2009.

Wright, I. J., Westoby, M., and Reich, P. B.: Convergence towards higher leaf mass per area in dry and nutrient-poor habitats has different consequences for leaf life span, J Ecol, 90, 534-543, 2002.

Wu, Y., Gong, W., Wang, Y., Yong, T., Yang, F., Liu, W., Wu, X., Du, J., Shu, K., Liu, J., Liu, C., and Yang, W.: Leaf area and photosynthesis of newly emerged trifoliolate leaves are regulated by mature leaves in soybean, J Plant Res, 131, 671-680, 2018.

Yue, X. and Unger, N.: The Yale Interactive terrestrial Biosphere model version 1.0: description, evaluation and implementation into NASA GISS ModelE2, Geosci Model Dev, 8, 2399-2417, 2015.

Zalles, V., Hansen, M. C., Potapov, P. V., Parker, D., Stehman, S. V., Pickens, A. H., Parente, L. L., Ferreira, L. G., Song, X.-P., Hernandez-Serna, A., and Kommareddy, I.: Rapid expansion of human impact on natural land in South America since 1985, Sci Adv, 7, eabg1620, 2021.

https://doi.org/10.5194/gmd-2022-227
Preprint. Discussion started: 19 September 2022

Geoscientific Model Development Discussions

Table 1. Summary of simulations.

Experiment [a]	Method	Thresholds [a] (x or y)	LMA format	LMA map	Optimal (a or a_{PFT})	Tests (a or a_{PFT})
YIBs-LMA	Mass-based	x=0.019	gridded	M2018	a=3.5 (Table S3)	five tests (a=2.5, 3, 3.5, 4, 4.5)
YIBs-LMA_PFT		x=0.019	PFT-specific	M2018	a=2.0 (Table S4)	five tests (a=2, 2.5, 3, 3.5, 4)
YIBs-LMA_T		x=0.006	gridded	M2018	a=3.0 (Table S5)	five tests (a=2, 2.5, 3, 3.5, 4)
YIBs-LMA_B2017		x=0.019	gridded	B2017	a=2.8 (Table S6)	five tests (a=2, 2.5, 2.8, 3, 3.5)
YIBs-S2007_adj	Area-based	8 values for y (Table S7)	/	/	8 values for a_{PFT} (Table S7)	40 tests (five each for 8 PFTs)

[a] Units of thresholds are nmol g^{-1} s^{-1} for x and nmol m^{-2} s^{-1} for y

[b] Units of key parameters are nmol^{-1} s g for a and nmol^{-1} m^{2} s for a_{PFT}

https://doi.org/10.5194/gmd-2022-227
Preprint. Discussion started: 19 September 2022

Geoscientific Model Development
Discussions
Open Access

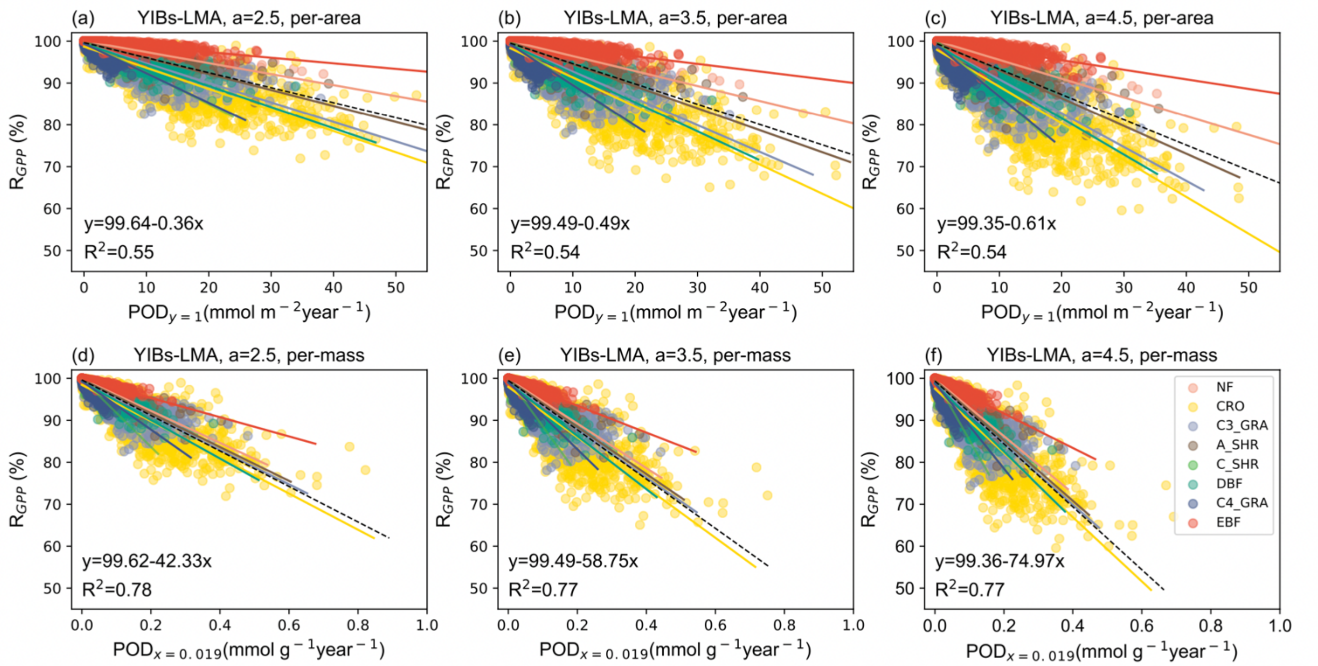

Figure 1. Area-based (top) or mass-based (bottom) DRRs for the YIBs-LMA experiment. Three tests from the YIBs-LMA experiment all adopt x=0.019 nmol g^{-1} s^{-1} and gridded LMA from M2018 with parameter a=2.5, 3.5, 4.5 nmol^{-1} s g, respectively. Each dot represents estimated POD-R_{GPP} ($POD_{y=1}$ for (a)-(c), $POD_{x=0.019}$ for (d)-(e)) at a grid with corresponding PFT. The PFT-specific regressions between area- or mass- based POD and R_{GPP} are displayed with solid lines shown in legend. Regression relationships of all PFTs are displayed in black dash line with coefficients of determination (R^2) denoted on each panel. Note the differences of ranges in x axis among PFTs. The YIBs-LMA experiment is summarized in Table 1.

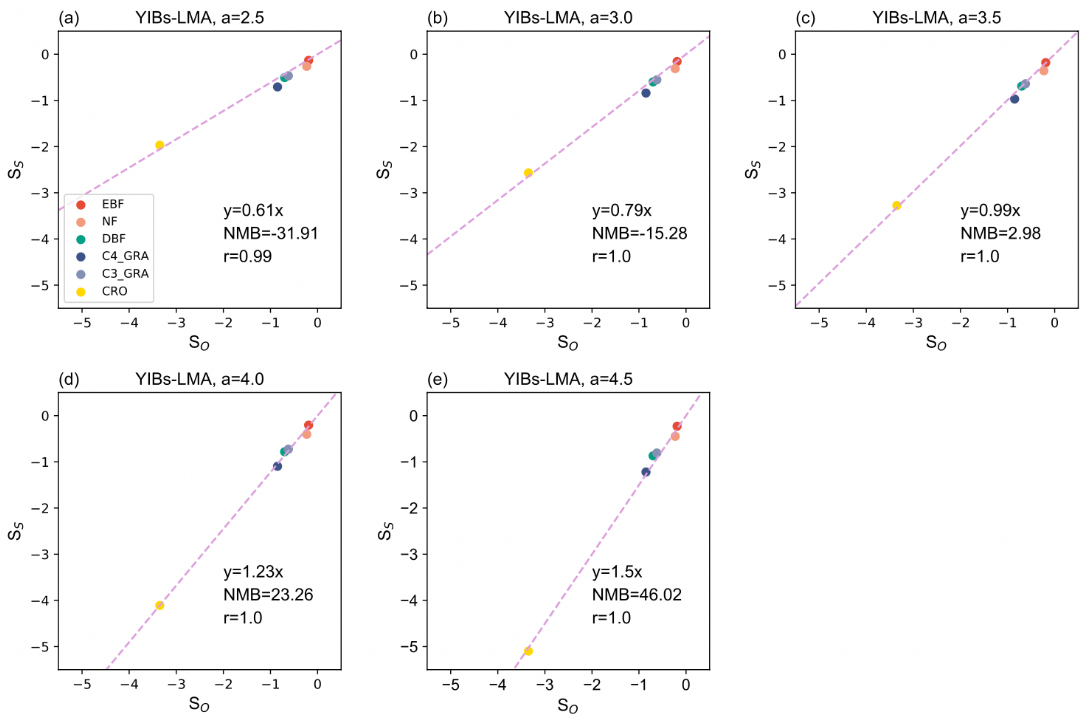

Figure 2. Comparison between S_O (% per mmol m^{-2}) and S_S (% per mmol m^{-2}) for the YIBs-LMA experiment. Five tests from the YIBs-LMA experiment all adopt x=0.019 nmol g^{-1} s^{-1} and gridded LMA from M2018 but with varied parameter a from (a) 2.5 to (e) 4.5 nmol^{-1} s g. S_O are from Table S1. S_S are derived as the slope between R_{GPP} and POD_y. The linear regression (dashed lines), normalized mean biases (NMB), and correlation coefficient (r) between S_S and S_O for varied PFTs are shown on each panel. The S_S and S_O of CRO are derived using $POD_{y=6}$ while other PFTs use $POD_{y=1}$. The YIBs-LMA experiment is described in Table 1.

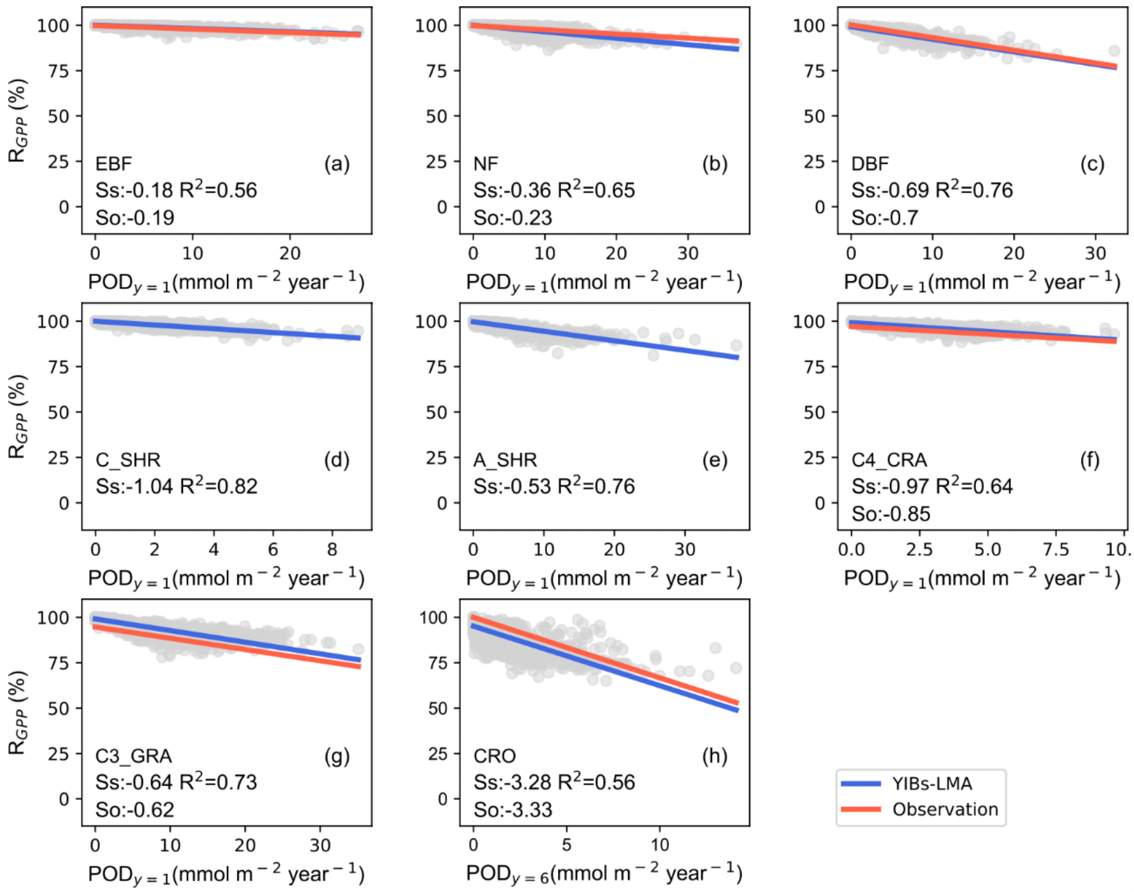

Figure 3. Comparisons of observed and simulated dose-response relationships. Simulated PFT-specific DRRs are derived from YIBs-LMA with gridded LMA from M2018, x=0.019 nmol g^{-1} s^{-1}, and a=3.5 nmol^{-1} s g. Each dot represents results from a gridcell with corresponding PFT. The regressions between relative GPP percentage (R_{GPP}) and leaf area-based stomatal O_3 uptake fluxes ($POD_{y=1}$ for natural PFTs and $POD_{y=6}$ for crops) are shown for observations (red, see Table S1) and simulations (blue) with slopes of DRRs denoted as *So* and *Ss*, respectively. S_O are missing for (d) cold and (e) arid shrubs. Coefficients of determination (R^2) of simulations are displayed in each panel. Note the differences of ranges in x axis among PFTs (PFTs are shown in Fig. S2).

https://doi.org/10.5194/gmd-2022-227
Preprint. Discussion started: 19 September 2022

Geoscientific Model Development
Discussions

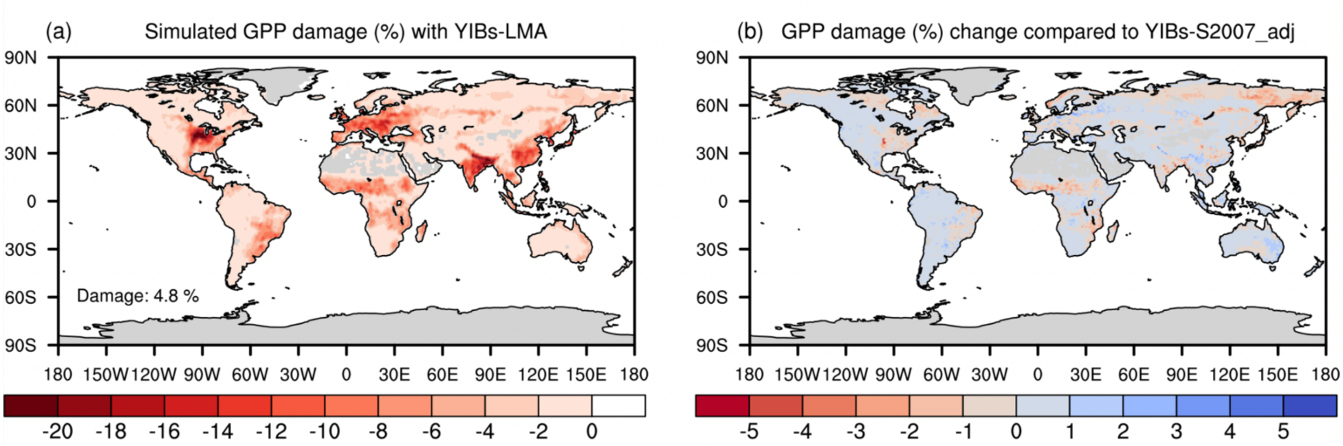

Figure 4. Global O_3 vegetation damage simulated with the LMA-based scheme. Results shown are the (a) GPP reduction percentages by O_3 simulated with the YIBs-LMA framework (gridded LMA from M2018, x=0.019 nmol g^{-1} s^{-1}, and a=3.5 nmol^{-1} s g), and (b) their differences compared to the predictions from YIBs-S2007_adj simulation. Blue (red) patches indicate the regions where damages predicted in YIBs-LMA are lower (higher) than those in YIBs-S2007_adj.

https://doi.org/10.5194/gmd-2022-227
Preprint. Discussion started: 19 September 2022

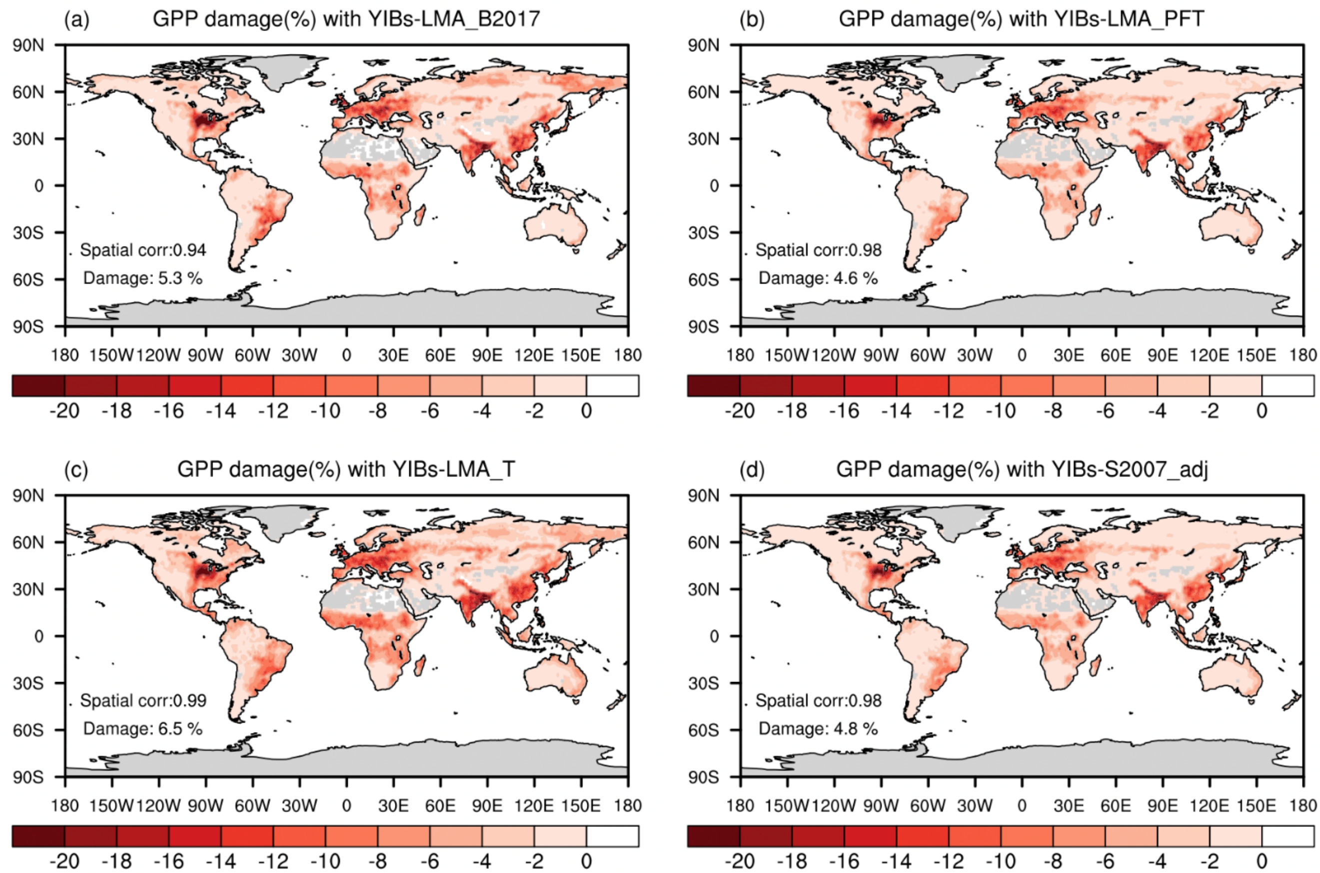

Figure 5. Global O_3-induced GPP reductions simulated in four supporting experiments. All damage maps are based on optimal parameters shown in Table 1. The spatial correlation coefficients between YIBs-LMA and these supporting simulations are shown on each panel as well as the global average damage percentage of each map. Simulations are described in Table 1.

https://doi.org/10.5194/gmd-2022-227
Preprint. Discussion started: 19 September 2022

Geoscientific Model Development
Discussions

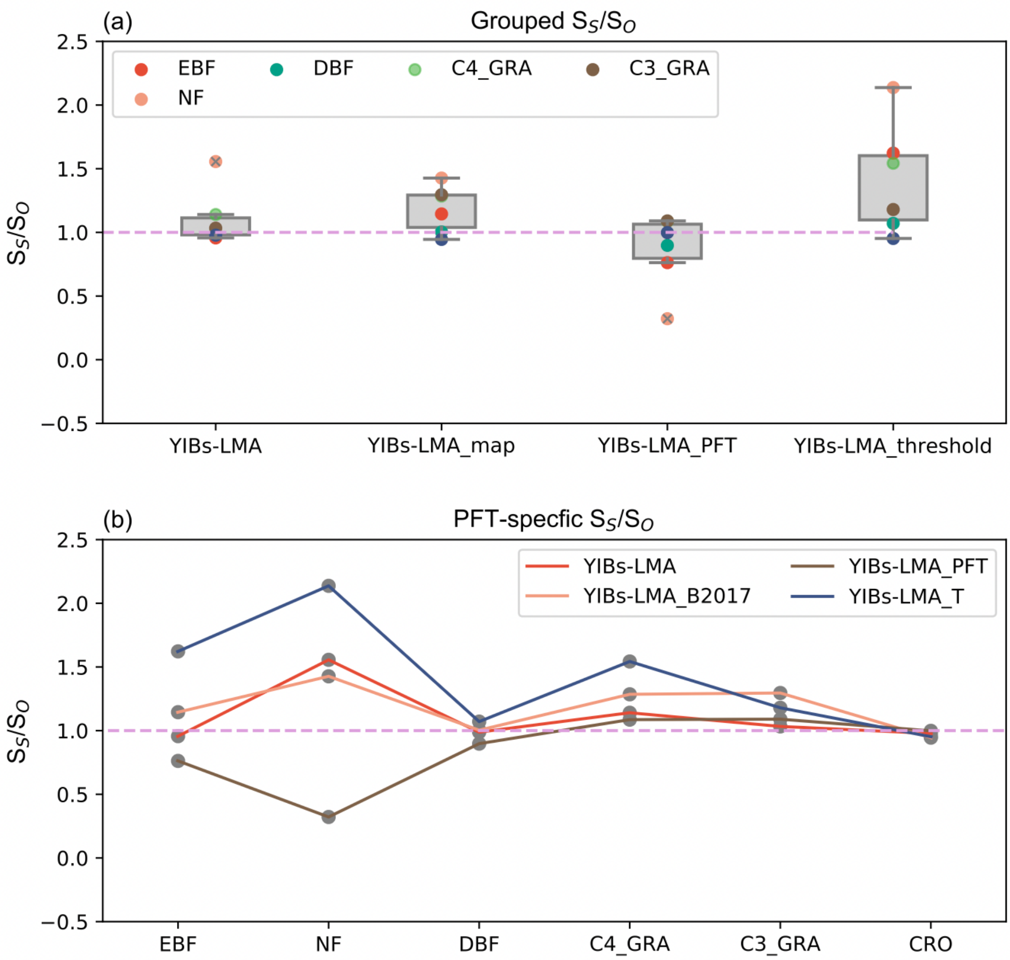

Figure 6. Comparison of S_S/S_O among supporting experiments. Individual ratios for (b) different PFTs are grouped to the boxplot in (a). All experiments adopt optimal parameters shown in Table 1.

https://doi.org/10.5194/gmd-2022-227
Preprint. Discussion started: 19 September 2022

Geoscientific Model Development
Discussions

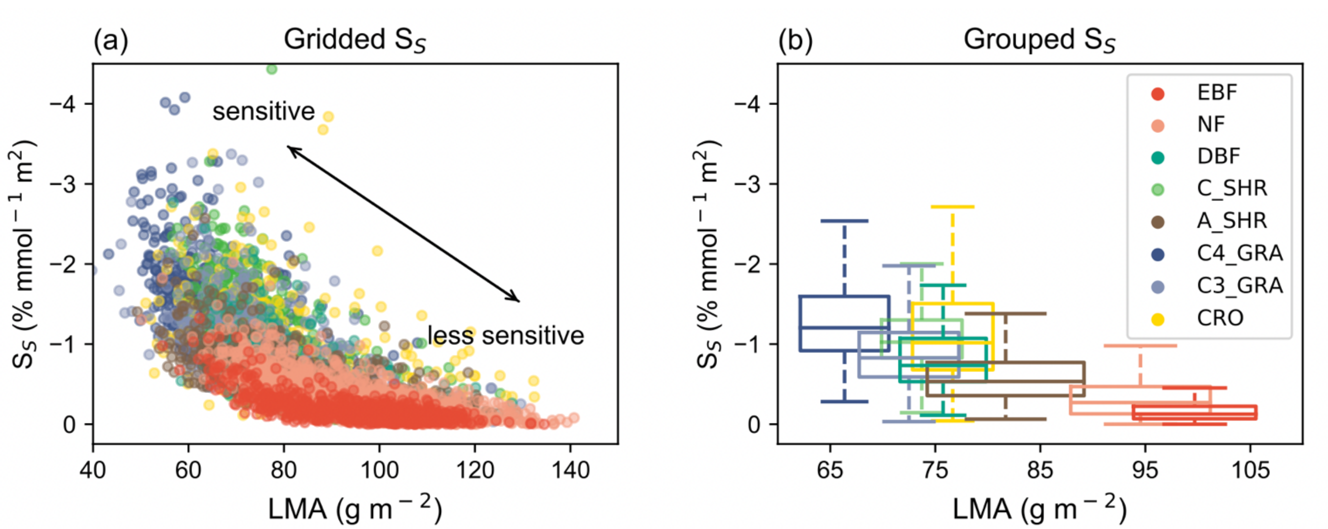

Figure 7. Relationships between O_3 sensitivity and LMA. (a) Simulated O_3 sensitivity (S_S) at each grid is compared with LMA for different PFTs. Gridded S_S is derived as GPP change per unit $POD_{y=1}$ from the YIBs-LMA simulation. Each point represents the value in a grid cell with a dominant PFT. (b) The PFT-level relationships between LMA and O_3 sensitivity are grouped as boxplots, which indicate the median, 25th percentile, and 75th percentile of y-axis variables within the same PFT. The width of boxplots represents one standard deviation of LMA for a specific PFT.

https://doi.org/10.5194/gmd-2022-227
Preprint. Discussion started: 19 September 2022

Geoscientific Model Development Discussions

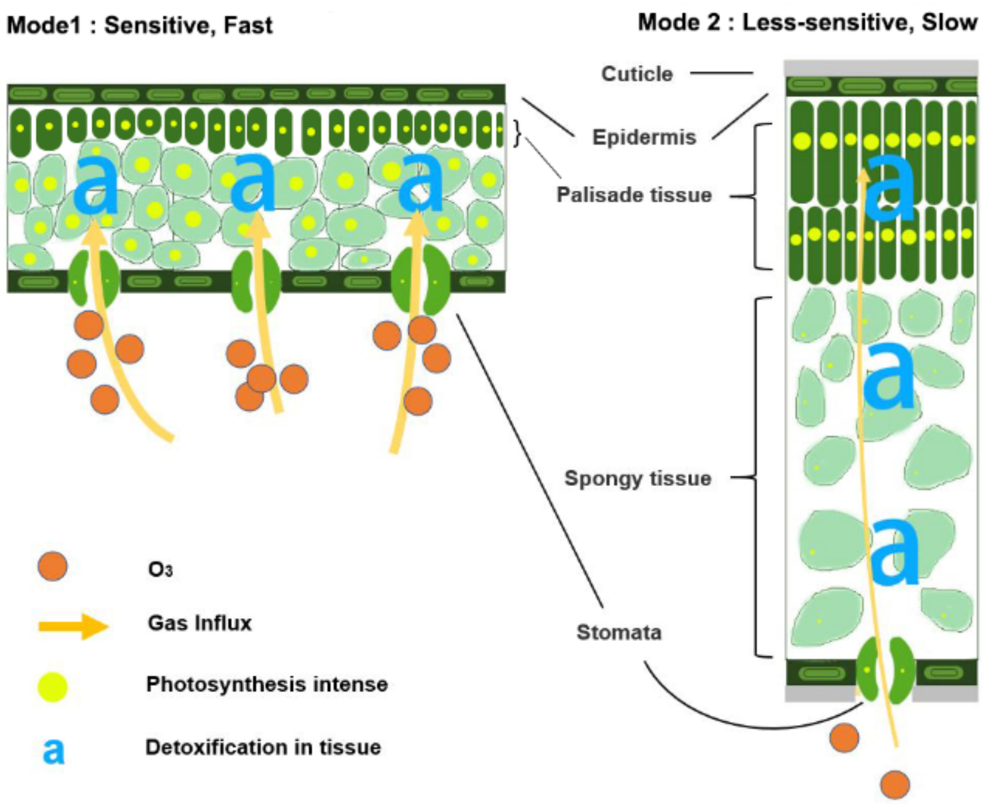

Figure 8. Illustration of the relationships between leaf trade-off strategy and its sensitivity to O_3